

FcεRI and Thy-1 domains have unique protein and lipid compositions[§]

Zurab Surviladze,* Kathleen A. Harrison,[†] Robert C. Murphy,[†] and Bridget S. Wilson^{1,*}

Department of Pathology,* University of New Mexico, Albuquerque, NM; and Department of Pharmacology,[†] University of Colorado at Denver and Health Sciences Center, Aurora, CO

Abstract Receptor activation leads to the dynamic remodeling of the plasma membrane. Previous work using immunoelectron microscopy showed that aggregated high-affinity receptor for immunoglobulin E (FcεRI) and aggregated Thy-1, a glycerophosphoinositol (GPI)-anchored protein, have distinct membrane distributions. We now report lipidomics analysis of FcεRI- and Thy-1-enriched vesicles obtained by magnetic bead isolation in the absence of detergent. Protein analyses show that FcεRI domains are enriched in receptors and associated signaling molecules, whereas Thy-1 domains are devoid of FcεRI subunits. Positive and negative ion electrospray mass spectrometry demonstrated that both domains retained a complex mixture of phospholipid classes and molecular species, predominantly glycerophosphocholine, glycerophosphoethanolamine (GPE), and sphingomyelin as well as glycerophosphoserine and GPI lipids. Analysis of total acyl groups showed that <50% of fatty acids in these domains are fully saturated, inconsistent with the recruitment of aggregated receptors or GPI-anchored proteins to liquid ordered domains. However, further analysis showed that FcεRI domains contain two times more sphingomyelin and a high ratio of cholesterol to total fatty acid content compared with Thy-1-enriched domains. Remarkably, plasmalogen glycerophosphoethanolamine phospholipids (plasmalogen GPE) were also 2.5–3 times more abundant in FcεRI domains than in the Thy-1 microdomains, whereas most diacyl GPE molecular species were equally abundant in the two domains.—Surviladze, Z., K. A. Harrison, R. C. Murphy, and B. S. Wilson. **FcεRI and Thy-1 domains have unique protein and lipid compositions.** *J. Lipid Res.* 2007. 48: 1325–1335.

Supplementary key words lipidomics • membrane microdomains • lipid rafts • immunoglobulin E receptor • glycerophosphoinositol-anchored proteins

Receptor activation leads to the dynamic remodeling of the plasma membrane, facilitating the initiation, propagation, and termination of intracellular signaling. This remodeling of the membrane includes both the redistribution of membrane proteins and the activation of a host

of enzymes that directly modify lipid substrates, including the phospholipases, inositol kinases, and phosphatases. Early insight into the importance of local lipid environments was provided by a series of studies using sucrose density centrifugation techniques to isolate detergent-resistant membranes (DRMs) from cell lysate preparations (1). The light fractions of these gradients are also often referred to as “lipid rafts,” reflecting their enrichment in cholesterol, sphingomyelins, and gangliosides (2) and in proteins that are covalently attached to lipid. Classical examples of the latter group include the Src and G-protein family proteins that are anchored to the inner leaflet of the lipid bilayer by acylation with fully saturated fatty acids (palmitate and/or myristate) (3–7). Glycerophosphoinositol (GPI)-anchored proteins in the outer leaflet, such as alkaline phosphatase and Thy-1, also float to the light fractions of density gradients (8, 9). Importantly, ligand-dependent shifts in receptor distributions in lipid raft fractions have supported the notion that movement in and out of these specific membrane domains is key to the signaling process (10–14).

Although these analyses have advanced the field, there are several limitations to lipid raft analysis by fractionation (15, 16). Compartments that were previously separate in native membranes can merge during the extraction process with detergents (17). Fractionation results are known to be dramatically altered by varying the concentration of Triton X-100 (18, 19), by the use of alternative detergents (11, 20, 21), or by the omission of detergent altogether (4, 22, 23). During the past decade, new biophysical and microscopic methods have been needed to estimate the size of putative microdomains, which are below the resolution (>300 nm) of conventional fluorescence microscopy (reviewed in Ref. 24). Several groups have proposed that

Abbreviations: DRM, detergent-resistant membrane; ESI, electrospray ionization; FcεRI, high-affinity receptor for immunoglobulin E; GPC, glycerophosphocholine; GPE, glycerophosphoethanolamine; GPI, glycerophosphoinositol; GPS, glycerophosphoserine; MβCD, methyl-β-cyclodextrin; MS/MS, tandem mass spectrometry.

¹To whom correspondence should be addressed.
e-mail: bwilson@salud.unm.edu

[§]The online version of this article (available at <http://www.jlr.org>) contains supplementary data in the form of three figures and two tables.

Manuscript received 13 November 2006 and in revised form 15 March 2007.

Published, JLR Papers in Press, March 26, 2007.
DOI 10.1194/jlr.M600485-JLR200

Copyright © 2007 by the American Society for Biochemistry and Molecular Biology, Inc.

This article is available online at <http://www.jlr.org>

rafts in resting cells are small, <70 nm (25, 26). Quantitative measurements of protein and lipid diffusion, including applications of fluorescence resonance energy transfer and single-particle tracking, have demonstrated that membrane components move at significantly slower rates than predicted from experiments in artificial membranes (27, 28). Membrane components also often appear to rapidly hop past diffusional barriers set up by interactions of membrane proteins and lipids with the cortical cytoskeleton (29) or possibly by transient residency in microdomains via a process of “dynamic partitioning” (30). This work has collectively demanded a revision of the classic view of randomly distributed membrane species, based upon the Singer-Nicolson model, to a new paradigm that has been described as a “dynamically structured mosaic model” (31). In recognition that many factors govern membrane organization, the term “lipid raft” has been replaced by many in the field with the term “membrane raft” (32).

Our group has sought alternative, detergent-free methods to evaluate the native distributions of receptors and their signaling partners. One powerful technique uses transmission electron microscopy of fixed, immunogold-labeled plasma membrane sheets, or “rip-flips” (33). By direct labeling of sheets prepared from resting cells, we found that clusters of high-affinity receptors for immunoglobulin E (FcεRI) and Thy-1 are very small (20–50 nm) in fixed membranes (34). Upon cross-linking, IgE receptors and a subset of their associated signaling proteins redistribute into large signaling patches (35, 36). Importantly, because the aggregation of IgE-bound receptors by polyvalent antigen is the physiological cue for FcεRI activation, these signaling patches closely approximate normal signaling architecture. Immune complexes have also been used by us and others (25, 34, 37) to aggregate GPI-anchored proteins on the surfaces of living cells, coalescing these putative raft markers into large aggregates that can be visualized by conventional fluorescence microscopy techniques. Electron microscopy of labeled membrane sheets demonstrated that aggregates of FcεRI and Thy-1 have distinct membrane distributions with little or no overlap (34).

In this work, magnetic beads were used to immunoprecipitate detergent-free membrane vesicles enriched in aggregated FcεRI or Thy-1 membrane proteins and their associated lipid environment. Although both sets of vesicles contain complex mixtures of phospholipids, there are remarkable differences between them. Cholesterol, traditionally associated with lipid raft integrity, constitutes 50% of the lipid content of FcεRI microdomains but <25% of the lipid associated with GPI-anchored aggregates. FcεRI microdomains also contain greater than two times more glycerophosphoethanolamine (GPE) plasmalogen and sphingomyelin species. These data suggest that the local lipid environment of receptors is both richer and less dependent on acyl chain saturation than proposed by the lipid raft hypothesis. These results are discussed in relation to prior lipidomics studies (38, 39) that analyzed the lipid composition of vesicles floating in bulk to the sucrose density light fractions with and without the influence of detergent.

Reagents and cell culture

RBL-2H3 cells were grown as adherent cultures in MEM (Gibco Life Technologies, Inc., Grand Island, NY) supplemented with 10% Hybrimax serum substitute (Sigma), fresh L-glutamine, and antibiotics. Where specified, cells were incubated overnight with 1 μg/ml murine dinitrophenol-specific IgE to prime IgE receptors. The IgE was affinity-purified from ascites using a trinitrophenol-conjugated Sepharose column.

For magnetic bead isolation, we used rabbit anti-IgE antibodies that were affinity-purified on a column composed of Sepharose conjugated to mouse IgE. For Western blotting of subunits of the FcεRI, mouse monoclonal anti-rat α(ER14) antibodies were generously provided by Dr. Reuben Siraganian (National Institutes of Health), anti-rat β monoclonal antibodies were a gift from Juan Rivera (National Institutes of Health), and rabbit polyclonal anti-γ antibodies were from Upstate Biological (Charlottesville, VA). Anti-OX7 antibodies were from BD Biosciences. Polyclonal anti-human FcεRI α was from US Biological (Swampscott, MA). Anti-Lyn and anti-Syk polyclonal antibodies were from Santa Cruz Biotechnology (Santa Cruz, CA). Colloidal gold secondary antibodies were from Amersham/GE Life Sciences (Piscataway, NJ). Rabbit anti-mouse IgG (Fcγ fragments) were from Jackson Laboratories. N-hydroxysuccinimide-biotin and avidin-HRP were from Sigma.

Membrane isolation

RBL-2H3 cells (60×10^6) were harvested with 1 mM EDTA in PBS. To aggregate surface GPI-anchored Thy-1 molecules, cells were washed, resuspended in Hanks' buffer, and incubated with OX-7 antibodies (1 μg/ml) at room temperature for 25 min. Cells were washed two times with Hanks' buffer and incubated with rabbit anti-mouse IgG (10 μg/ml) for 10 min at 37°C. To aggregate surface FcεRI, IgE-primed RBL cells were harvested with EDTA-PBS, washed, resuspended in Hanks' buffer, and incubated with anti-IgE polyclonal antibodies (5 μg/ml) for 3 min at 37°C. In both cases, cells were transferred to an ice bath, followed by the addition of 10 ml of ice-cold Hanks' buffer. Cells were collected by centrifugation at 4°C, washed with cold Hanks' solution, and resuspended in 10 ml of cold hypotonic buffer (10 mM Tris, pH 7.5, 10 mM KCl, 5 mM MgCl₂, and 1 mM EGTA) supplemented with 1 mM vanadate and protease inhibitors. All tubes and pipette tips were rinsed with chloroform-methanol (2:1) solution to remove any lipid contaminants and other organic solvent-soluble contaminants that interfere with mass spectrometric analyses. Fatty acid-free BSA (Sigma) was used for the preparation of Hanks' buffer. For the preparation of negative controls, the same number of RBL cells were harvested, washed, and resuspended in hypotonic buffer.

Homogenization steps were performed on ice. Cells in hypotonic buffer were passed through a 26 g needle five times. Broken cells were then passed through a ball-bearing-style cell cracker (15–20 strokes), followed by 20 s of sonication. Unbroken cells were sedimented by centrifugation (600 g for 10 min at 4°C) and discarded. The supernatant was centrifuged at 16,000 g for 45 min at 4°C. The resulting membrane-enriched pellet fraction was resuspended in 3 ml of cold PBS and again sonicated for 15 s. Aggregated material was removed by low-speed centrifugation for 10 min. Combined supernatants were used for immunoprecipitation of microdomains. An equal amount of sheep anti-rabbit IgG-Dynabeads M-280 (DynaL Biotech) was added to each sample. Samples were diluted up to 4 ml with cold PBS and incubated overnight at 4°C on a wheel rotator. Magnetic beads were washed five times with 3 ml of cold PBS. For protein analysis, beads were

resuspended in loading buffers appropriate for one-dimensional or two-dimensional electrophoresis. For lipid analysis, beads were transferred into the glass vials and treated with 100 μ l of methanol-water (2:1). Vials were closed under nitrogen and stored at -20°C until lipid extraction.

Lipid extraction

Lipids were recovered from the magnetic beads by the addition of 400 μ l of ethanol containing appropriate internal standard(s) for subsequent procedures. Ethanol was used rather than CH_2Cl_2 /methanol because the polystyrene beads are not resistant to CH_2Cl_2 . Ethanol extraction of phospholipids has been described (40). The beads and solvent were vortexed and centrifuged to pellet the beads, and the supernatant was drawn off with a pipette.

Cholesterol analysis

For cholesterol analysis, 50 ng of [$^2\text{H}_6$]cholesterol internal standard (97 atom% excess; Cambridge Isotope Laboratories, Inc., Andover, MA) was added to the ethanol extraction. Aliquots (100 μ l) were transferred to a screw-cap glass tube, dried under N_2 , and resuspended in 50 μ l of acetonitrile plus 50 μ l of *N,O*-bis(trimethylsilyl)-trifluoroacetamide. The tubes were heated to 60°C for 20 min to convert the free hydroxy to the trimethylsilyl ether derivative for GC-MS analysis. Positive ion electron ionization mass spectrometry was used to monitor m/z 369 and 374 (corresponding to the $[\text{M-TMSOH}]^+$ ions for endogenous cholesterol and deuterium-labeled [$^2\text{H}_6$]cholesterol internal standard, respectively). Quantitation was performed by comparison of the chromatographic peak area ratio of m/z 369 to m/z 374 with a seven point standard curve (1.6–5,000 ng of cholesterol). Conditions for GC-MS were as follows: 30 m \times 0.25 mm ZB-1 (Phenomenex, Torrance, CA); 0.1 μm film thickness; temperature programmed from 150°C to 300°C at $20^{\circ}\text{C}/\text{min}$, then held at 300°C for 2.5 min; quadrupole mass spectrometer (TRACE DSQ; Thermo-Finnigan, San Jose, CA); 70 eV electron ionization; source temperature of 200°C ; and helium used as the carrier gas at 1.5 ml/min.

Fatty acid analysis

Total fatty acid analysis was performed after base hydrolysis of a 100 μ l aliquot of the ethanol supernatant. Stable isotope-labeled palmitic acid ($^{13}\text{C}_4$ 16:0) (97 atom% excess; Cambridge Isotope Laboratories), stearic acid ($^2\text{H}_3$ 18:0) (98 atom% excess; Cambridge Isotope Laboratories), oleic acid ($^2\text{H}_2$ 18:1) (97 atom% excess; Cambridge Isotope Laboratories), and arachidonic acid ($^2\text{H}_8$ 20:4) (96 atom% excess; Cayman Chemical, Ann Arbor, MI) served as internal standards. Base hydrolysis was accomplished by the addition of 100 μ l of 1 N NaOH and saponification for 30 min. Acidification of the reaction with HCl followed by extraction with iso-octane recovered the total fatty acids in the lipid extract. Fatty acids were converted to pentafluorobenzyl esters (1% pentafluorobenzyl bromide, 1% diisopropylethylamine in acetonitrile, 20 min, room temperature) for analysis by negative ion chemical ionization GC-MS with selected ion monitoring of the $[\text{M-PFB}]^-$ ions (41). Procedural blanks were obtained by ethanol extraction of magnetic beads that had not been exposed to cells and were used alongside the samples to correct for background levels of fatty acids. Quantitation of the fatty acids was determined by comparisons of the peak area ratios of the fatty acid $[\text{M-PFB}]^-$ ions with the $[\text{M-PFB}]^-$ ions of their internal standards on a seven point standard curve constructed for each fatty acid (0.32–1,000 ng range). The GC-MS conditions were the same as those used for cholesterol analysis except that negative ions were monitored and methane was used as the reagent gas.

Phospholipid analysis

Lipid extracts were first treated by adding 200 ng of 17:0a/17:0 GPE internal standard (Avanti Polar Lipids, Alabaster, AL), then analyzed using normal-phase HPLC-electrospray ionization (ESI)-MS and tandem mass spectrometry (MS/MS) phospholipid polar head group scans, with 90% split to a fraction collector for further analyses (42). Separation of the phospholipid classes was achieved using a 4.6 mm \times 250 mm silica column (Ultremex 5u; Phenomenex) with a gradient of hexane-isopropanol-water containing 1 mM NH_4OAc . Gradient elution proceeded from 47% B applied to the column for 6 min, then increased to 100% B over 20 min and held for 30 min, where solvent A = 3:4 hexane-isopropanol and solvent B = 3:4:0.7 hexane-isopropanol-water and 1 mM NH_4OAc . The flow rate was maintained at 1 ml/min throughout. Under these conditions, neutral lipids (including cholesterol) elute first, followed by GPI, GPE, glycerophosphoserine (GPS), glycerophosphocholine (GPC), and sphingomyelin. Multiple scans were performed throughout the analyses. GPI was detected using negative ESI. GPE was detected by positive ion ESI as well as the neutral loss of 141u (NL 141). In the NL 141 scan, the phosphoethanolamine polar head group left as a neutral fragment, leaving the charge on the remainder of the molecule. This procedure selectively detected the diacyl glycerol ions and severely discriminated against plasmalogens and alkyl ether

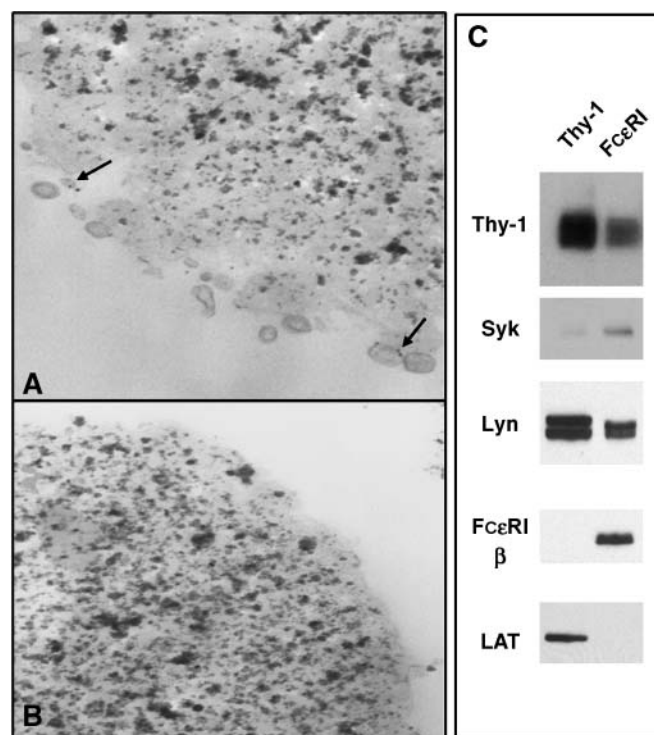


Fig. 1. A: Cross-sectional view of a magnetic bead coated with anti-IgE antibodies and bound to vesicles containing IgE-bound receptors. Images were acquired by transmission electron microscopy of ultrathin sections. Arrows point to anti-IgE gold used to confirm the presence of high-affinity receptor for immunoglobulin E (FcεRI) in bound vesicles. B: Control bead that was incubated with membrane fractions, but no primary antibody, is clean. C: After isolation using anti-IgE or anti-Thy1 antibodies, vesicles were lysed in Laemmli buffer, and proteins were separated by SDS-PAGE, transferred to nitrocellulose, and blotted to demonstrate unique subsets of proteins in the two vesicle populations. Results are representative of three separate experiments.

molecular species of GPE (43). GPS was detected by the neutral loss of 185u, which corresponded to the loss of phosphoserine from the protonated molecular ions of GPS species. GPC and sphingomyelin were detected by monitoring the precursors of m/z 184, the phosphocholine ion. Analyses were performed on an Applied Biosystems (Framingham, MA) API 3000 triple quadrupole mass spectrometer. The ion spray voltage was 4,600 V, declustering potential was 70 V, collision energy was 30 eV, and collisional gas setting was 8.

Analysis of GPE species using isotope-tagged derivative

Precise determination of differences in GPE molecular species composition was carried out using a stable isotope dilution strategy after isolation of this class of phospholipids from the original ethanol extract. For these experiments, the remainder of the GPE fractions collected during LC-MS were derivatized with the isotope-tagged *N*-methylpiperazine *N*-hydroxy succinimide ester reagent (iTRAQ derivative; Applied Biosystems) as described (44) The GPE from the control (no primary antibody added) was derivatized with the 115-isotope-tagged reagent, the

Thy-1 GPE was derivatized with the 117-isotope-tagged reagent, and the Fc ϵ RI GPE was derivatized with the 114-isotope-tagged reagent. The isotope-tagged samples were then combined and analyzed by nanoflow ESI-MS/MS/MS. The MH^+ ions were chosen from a survey scan of the precursors of m/z 286. These MH^+ ions were decomposed in the collision cell (Q2), and their common product ion (m/z 286, which contains the isotope tags) was stored in the linear ion trap (Q3-linear ion trap) and collisionally decomposed to produce reporter ions, which were mass analyzed and detected. The peak areas for each reporter ion (m/z 114 for Fc ϵ RI, m/z 115 for the control, and m/z 117 for Thy-1) were divided by the peak area of the reporter ion for the 17:0a/17:0 GPE internal standard to correct for sample losses. Analyses were performed on an Applied Biosystems API 4000 triple quadrupole-linear ion trap mass spectrometer equipped with the Advion Nanomate (Ithaca, NY) for nanospray ionization sample introduction. The lipids were dissolved in methanol:AcCN: 10 mM NH_4OAc (60:20:20) and diluted so that the internal standard concentration was ~ 20 $\mu g/\mu l$. The API 4000 was operated with declustering potential of 80 V, high collisional gas setting, collision energy of 40 eV, and ion trapping time of 300 ms. The

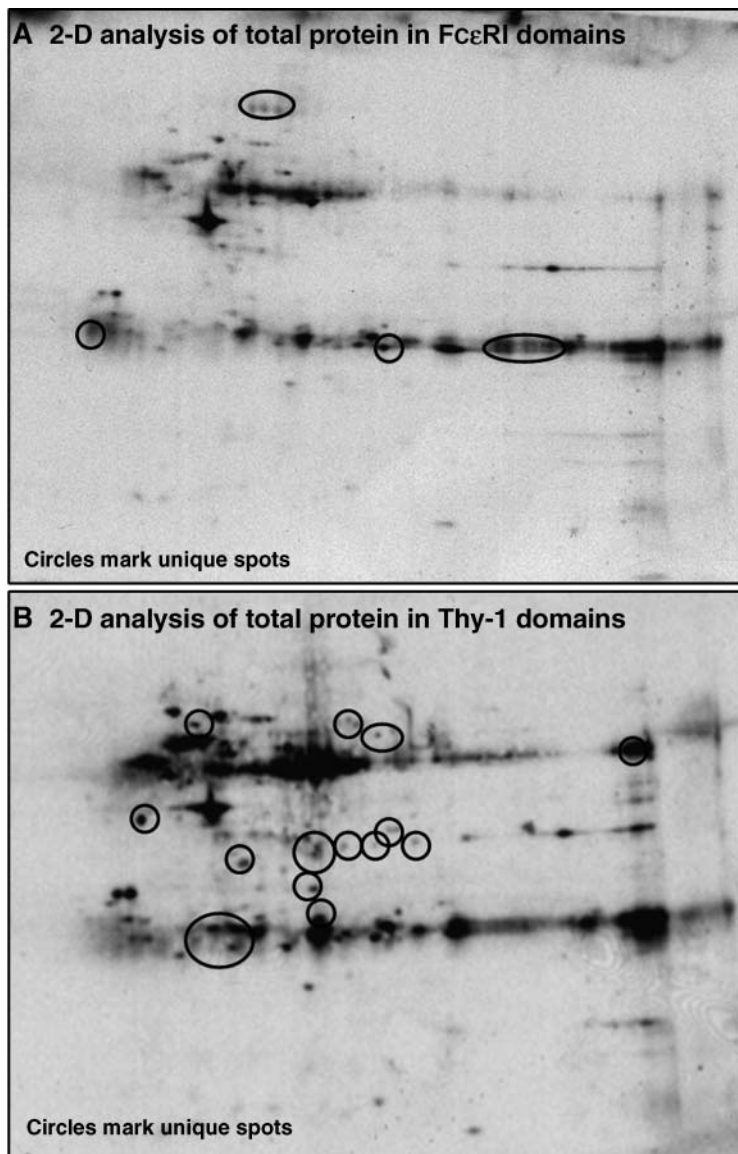


Fig. 2. Two-dimensional (2-D) gel electrophoresis analysis of proteins in the Fc ϵ RI microdomains (A) or Thy-1 microdomains (B). After electrophoresis and transfer of proteins to nitrocellulose, blots were stained for total protein. Circles highlight unique protein spots in each of the two membranes. Results are representative of two separate experiments.

Nanomate was operated with a voltage of 1.33 kV and gas pressure of 0.13 p.s.i.

RESULTS

Harder and Kunh (45) previously described a novel approach to the isolation of plasma membrane fragments. Working with Jurkat T-cells, they incubated cells with anti-CD3-coated magnetic beads, followed by mechanical disruption. Membrane recovered on the magnetic beads was 50-fold enriched for T cell receptor compared with the bulk membrane. We modified this technique to isolate very small patches of RBL membranes representative of domains surrounding aggregates of either FcεRI or the GPI-anchored protein Thy-1. This detergent-free strategy yielded a highly enriched preparation of right side out membrane vesicles. The protocol was initiated by incubating live RBL cells with rabbit polyclonal antibodies to IgE (which cross-link IgE-primed FcεRI) or a combination of

mouse monoclonal anti-Thy-1 antibodies and polyclonal anti-mouse secondary antibodies (which aggregate GPI-anchored surface Thy-1 molecules). After incubation, cells were lysed at 4°C by a combination of mechanical disruption and sonication. Vesicles enriched in FcεRI or Thy-1 aggregates were then immunisolated on magnetic beads. Dynal beads were chosen for their relatively smooth surface, as characterized previously by Saucan and Palade (46). The size and specificity of bound vesicles was determined by labeling immunisolated FcεRI vesicles with anti-IgE immune complexes conjugated to 10 nm colloidal gold, glutaraldehyde fixation, dehydration, and embedding in Epon. Ultrathin sections were prepared and examined by transmission electron microscopy. **Figure 1A** shows a cross-sectional view of a magnetic bead whose surface was coated with many small vesicles (diameter < 100 nm) that label specifically with gold directed at IgE bound to surface receptors (arrows). Vesicles of similar size and purity were isolated using anti-Thy1 reagents (data not shown). **Figure 1B** shows a cross-sectional view of a magnetic bead

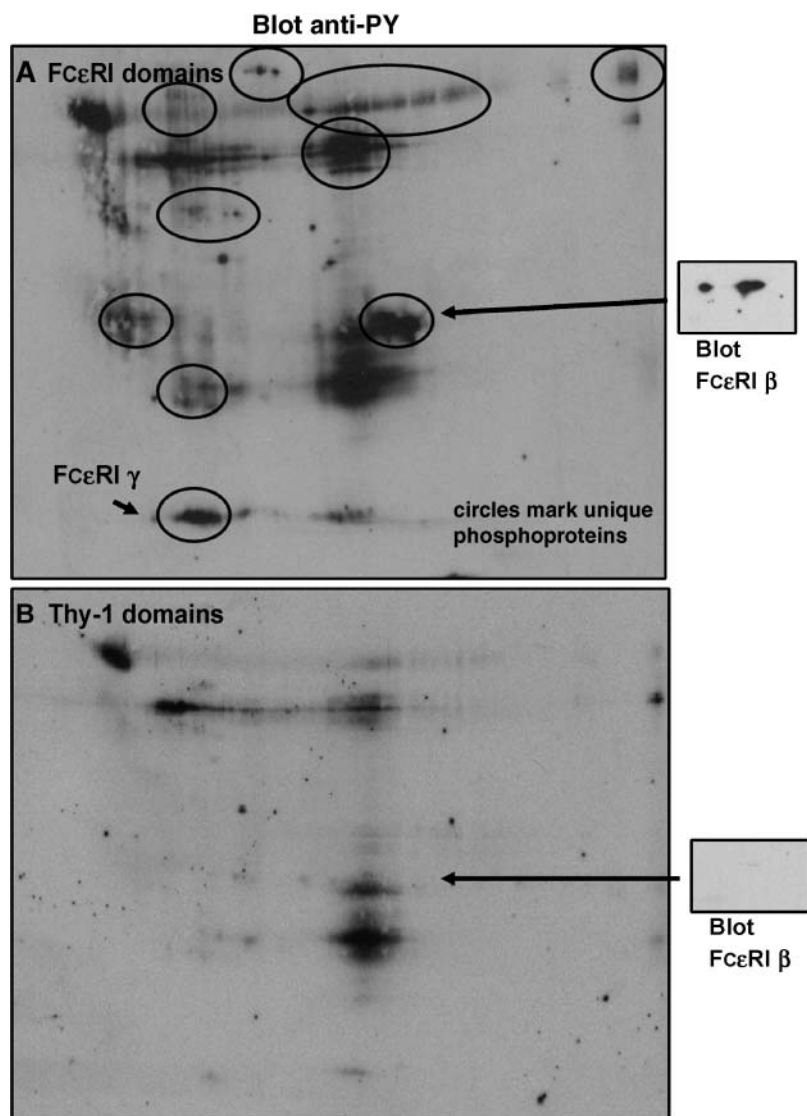


Fig. 3. Two-dimensional gel electrophoresis analysis of tyrosine-phosphorylated proteins in the FcεRI microdomains (A) or Thy-1 microdomains (B). After electrophoresis and transfer of proteins to nitrocellulose, membranes were probed with HRP-conjugated anti-phosphotyrosine antibodies followed by ECL development. Circles in A highlight unique phosphoproteins in the FcεRI microdomains. Stripped membranes were also probed with specific antibodies to the FcεRI β and γ subunits (side boxes), demonstrating that only FcεRI microdomains contain IgE receptor subunits. Results are representative of two separate experiments.

that was incubated with lysates in the absence of primary antibodies. These control beads are clean of bound vesicles. A diagram of the isolation strategy is provided in supplementary Fig. 1.

Magnetic bead-isolated vesicles isolated using anti-IgE or anti-Thy-1 antibodies have distinct protein compositions

As an initial characterization of the two immunisolated vesicle preparations, vesicles were lysed and boiled in Laemmli buffer for one-dimensional separation of proteins by SDS-PAGE. Proteins in the gels were electrophoretically transferred to nitrocellulose, followed by immunoblotting for a subset of mast cell proteins expected to differentially segregate into FcεRI and Thy-1 microdomains. The results are shown in Fig. 1C, where FcεRI vesicles are shown to exclusively contain the FcεRI β subunit and to be enriched in the important FcεRI-coupled tyrosine kinase, Syk. Small amounts of Thy-1 were associated with FcεRI microdomains, as expected from earlier electron microscopy data showing that singlets and small clusters of unaggregated Thy-1 were well dispersed and not restricted from primary receptor signaling domains (34). Small amounts of Lyn were also present, consistent with Lyn's progressive dissociation from FcεRI signaling complexes after it has phosphorylated β and γ subunit Immunoreceptor Tyrosine-based Activation Motifs (35). In contrast, vesicles containing immunisolated Thy-1 aggregates have very little Syk, no FcεRI β subunit, and high levels of the dually acylated Lyn tyrosine kinase. Thy-1 vesicles also contain the palmitoylated adaptor protein Linker for Activation

of T Cells (LAT), previously shown by electron microscopy to be coclustered with the GPI-anchored protein after antibody-induced aggregation of Thy-1 (34).

Two-dimensional gel electrophoresis was next used to more fully characterize the protein composition of the two vesicle preparations. Results in Fig. 2 show blots stained for overall protein by incubating membranes in borate buffer containing N-hydroxysuccinimide-biotin, which labels free amine groups. Protein spots on the membranes were visualized by sequential incubation with avidin-HRP and chemiluminescence solution, followed by film development. Figure 2A represents total proteins in FcεRI-enriched domains and Fig. 2B represents total proteins in Thy-1-enriched domains. Spots representing unique proteins in each preparation are circled, illustrating that although there is some overlap in protein composition, there are also significant differences in overall protein contents.

Blots shown in Fig. 3 were probed with anti-phosphotyrosine antibodies. FcεRI domains (Fig. 3A) contain abundant tyrosine-phosphorylated proteins, including the β and γ subunits of the receptor. Cross-linking of Thy-1 leads to the association of a smaller subset of tyrosine-phosphorylated proteins with Thy-1 domains (Fig. 3B). Specificity is again shown by the lack of the β subunit of the IgE receptor in the Thy-1 domains (boxes at right).

Magnetic bead-isolated vesicles contain a complex mixture of phospholipids

Nanoflow electrospray mass spectrometry was used to initially survey the phospholipids associated with the im-

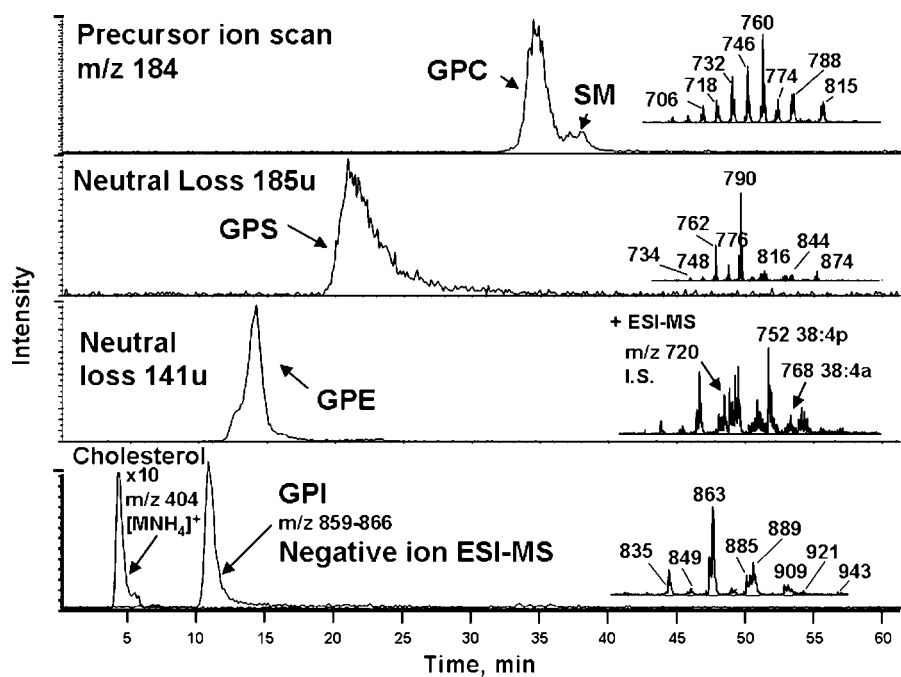


Fig. 4. Normal-phase HPLC-MS analysis of a sample of lipids from the IgE receptor microdomain, demonstrating sequential elution of cholesterol (and other neutral lipids) and glycerophosphoinositol (GPI), glycerophosphoethanolamine (GPE), glycerophosphoserine (GPS), and glycerophosphocholine (GPC) with sphingomyelin (SM). ESI, electrospray ionization.

munisolated vesicles. Analysis of the crude extracts by both positive and negative ion nanoflow ESI revealed an impressive range of phospholipid classes and molecular species (see supplementary Fig. III). All major phospholipid groups (GPC, GPE, GPI, and GPS) were well represented in vesicles enriched in both FcεRI and Thy-1 (see supplementary Table I). As a control for the expectation that the unoccupied bead surface would absorb some lipids, we also analyzed beads that were incubated with vesiculated RBL membranes in the absence of primary antibodies (see supplementary Table I). Although ~50% less abundant than the immunisolated lipids, sensitive mass spectrometry analysis showed that a large number of species in the RBL cell lipidome were represented.

Having established the complexity of the phospholipids isolated in the immunisolated vesicles, we next performed normal-phase HPLC-MS/MS analyses to evaluate the relative abundances of the phospholipids in the two different microdomains (Fig. 4). There were no major differences in relative abundances of the GPC, GPS, or GPI molecular species between the FcεRI and Thy-1 microdomains (data not shown). However, the HPLC-MS/MS analyses of GPE phospholipid species indicated significant differences between the two microdomains, particularly for the plasmalogen (plasmalogen) GPE species (Fig. 5). We used an isotope-tagged derivative to precisely determine relative differences in the molecular species between microdomain samples.

FcεRI domains are enriched in GPE plasmalogens

The utility of the isotope-labeled *N*-methylpiperazine reagent (see supplementary Fig. IIB) is based upon its rapid and quantitative reaction with the primary amine of GPE and the ability to generate isotope-tagged yet isobaric derivatives that could be decoded by a MS³ strategy. MS/MS of derivatized GPE species gave rise to an ion at *m/z* 286. GPE lipids isolated from the control and each of the two samples were derivatized with methylpiperazine tags that differed only in the number of stable isotopes in the reporter portion of the derivative. The samples were combined and analyzed using nanospray ionization with MS³ analysis of the derivative-specific ion, *m/z* 286. For each molecular species [M+H]⁺, the common ion *m/z* 286 was further decomposed in a second collisional activation step (MS³) to yield the reporter ions *m/z* 114, 115, and 117 (Fig. 6). The abundance of each reporter ion was then used as a direct measure of the relative abundance of each GPE species in the two microdomain preparations as well as the control sample. The internal standard GPE (17:0/17:0 GPE) was also analyzed by this method (Fig. 6, inset), and the ratio of the reporter ion abundance for this molecular species was used to normalize the reporter ions derived from each isotope-tagged GPE molecular species.

One of the most abundant diacyl GPE species was 18:1/18:1 GPE (*m/z* 744, positive ions; Fig. 5), detected at *m/z* 888 when derivatized with the isotope-tagged reagent. Decoding of this species (Fig. 6) suggested that its levels were very similar in abundance in all three samples compared with the internal standard isotope. The major diacyl

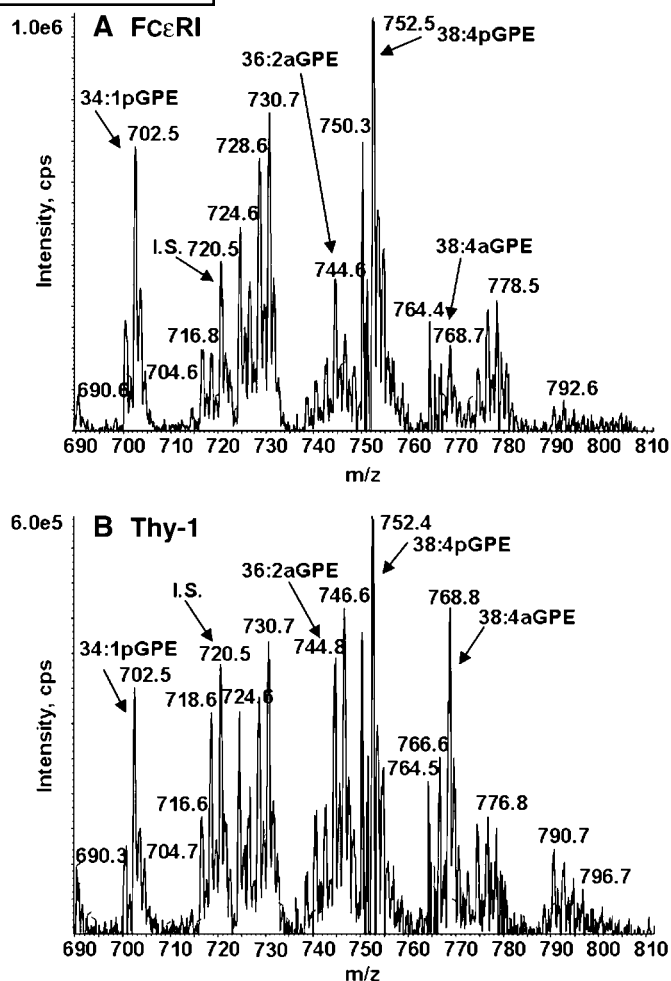


Fig. 5. Positive ion ESI mass spectra from GPE of the FcεRI microdomain (A) and the Thy-1 microdomain (B). *m/z* 720 corresponds to the 17:0/17:0 GPE internal standard (I.S.).

GPE species that contained arachidonic acid (38:4a; Fig. 6) was more abundant in the Thy-1 vesicles. In sharp contrast, the plasmalogen GPE molecular species (34:1p and 38:4p; Fig. 6) were >2-fold more abundant in the FcεRI-enriched vesicles relative to control magnetic beads and Thy-1 immunisolated vesicles.

Analysis of all GPE molecular species measured using the isotope-tagging method revealed that plasmalogen GPE molecular species on average were 2.7 ± 0.8 times more abundant in the IgE receptor microdomains than in the Thy-1 microdomains (Fig. 7). Conversely, the diacyl GPE species were somewhat more abundant in the Thy-1 microdomains than in the IgE receptor microdomains.

Cholesterol and fatty acyl composition

Analysis of cholesterol content revealed another striking difference in the two isolated vesicle preparations. Results of four independent experiments (Fig. 8) revealed that the cholesterol content of FcεRI-enriched vesicles was markedly higher, with a ratio of 0.8–1.2 for cholesterol to total fatty acid content. The lipid content

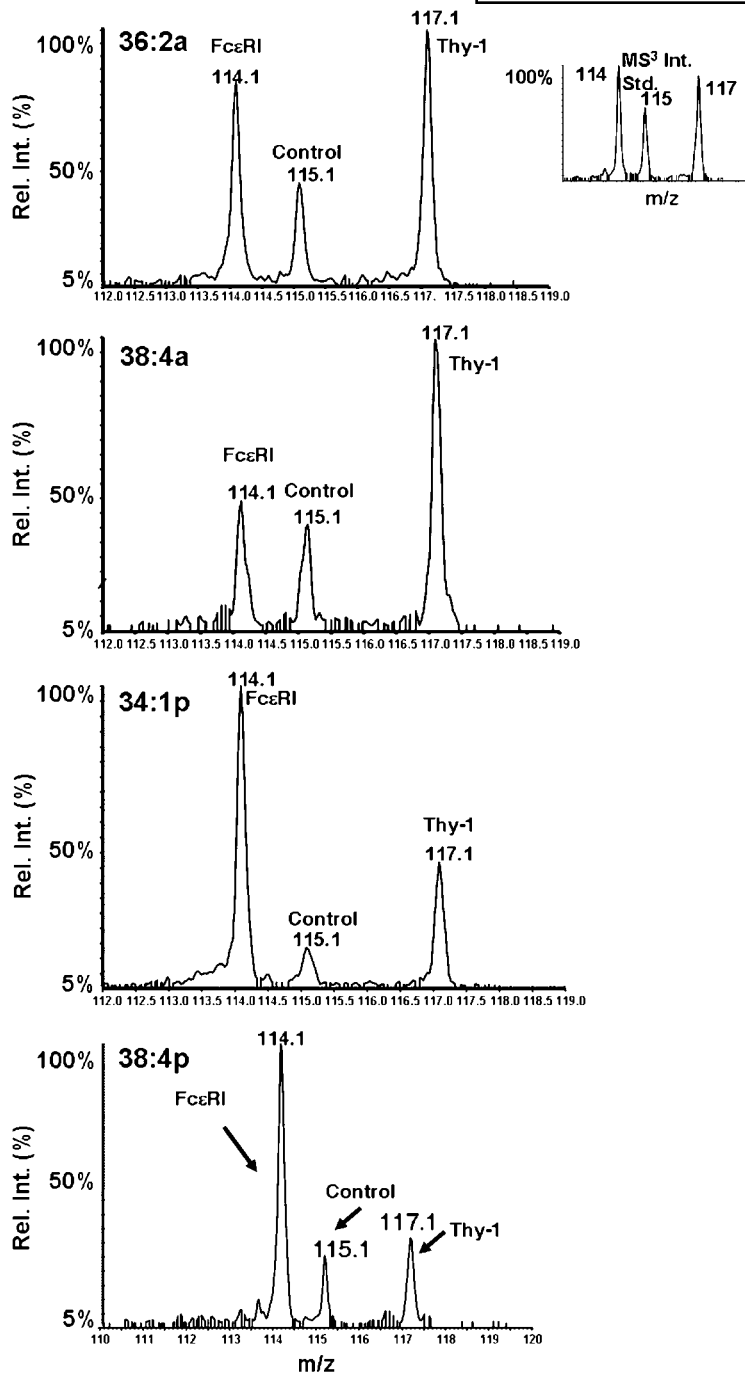


Fig. 6. Use of iTRAQ reagent to compare the levels of diacyl and vinyl ether (plasmalogen) phospholipids in the FcεRI and Thy-1 microdomains. GPEs in each of the sample preparations were isolated and modified with a distinct iTRAQ isotope tag, as described in Materials and Methods and outlined in supplementary Fig. II. Control samples were modified with the 115.1 tag, FcεRI microdomains were modified with the 114.1 tag, and Thy-1 microdomains were modified with the 117.1 tag. Representative results of these analyses are shown for the relative abundance of the 36:2 diacyl species, the 38:4 diacyl species, the 34:1 plasmalogen species, and the 38:4 plasmalogen species. Rel. Int., relative intensity.

of vesicles enriched in the putative raft marker, Thy-1, had a much lower cholesterol content, with ratios of cholesterol to total fatty acid of 0.3–0.5 in the four measurements. These results suggest that receptor microdomains are particularly dependent upon cholesterol for their integrity.

Total fatty acids derived from all phospholipids revealed that only 46% of fatty acids in the FcεRI-enriched vesicles were fully saturated (see supplementary Table I). Fully saturated species in Thy-1-enriched vesicles were slightly less (42%; see supplementary Table I). Thus, neither microdomain was predominantly composed of saturated fatty acyl-substituted phospholipids that form liquid ordered

domains in artificial membranes. Both immunisolated preparations contained roughly twice as much fatty acids as controls.

FcεRI domains are enriched in sphingomyelin

The relative abundance of sphingomyelin lipids was also measured in the Thy-1 and FcεRI samples (see supplementary Table II). All samples were normalized to internal standards, and values for three GPC molecular species are shown for comparison. As shown, all three major sphingomyelin molecular species were >2-fold more abundant in FcεRI domains compared with Thy-1 domains. The 32:0e GPC was also enriched in FcεRI microdomains. In con-

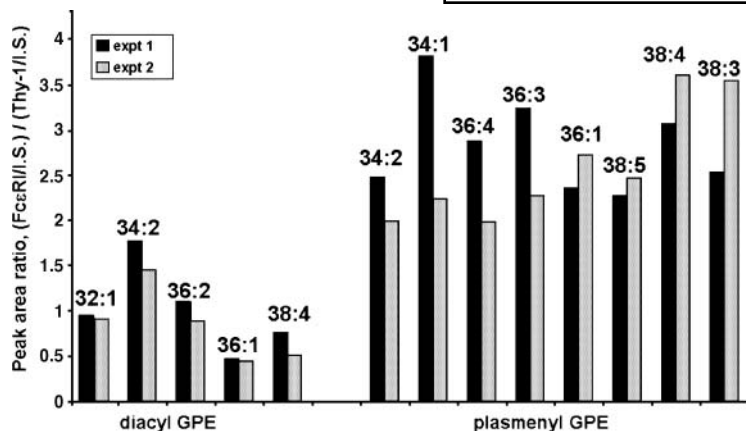


Fig. 7. Summary of the levels of ester and vinyl ether phospholipids measured in two replicate experiments, expressed as a ratio of relative abundances normalized to the GPE internal standard (I.S.) in FcεRI microdomains to those in Thy-1 microdomains.

trast, the 34:1a and 32:1e GPC species were slightly more abundant in the Thy-1 microdomains.

DISCUSSION

The rapidly advancing field of cellular lipidomics promises to shed light on the complexity and organization of the lipid bilayer (47). Here, sophisticated mass spectrometry techniques were used to analyze the lipid composition of immunisolated membrane microdomains prepared in the absence of detergent. This is an important distinction, because previous attempts to further analyze the composition of the lipid environment of FcεRI during the signaling process have been limited to the DRMs of RBL cells (38). The extent to which isolated DRMs reflect the composition of native membrane domains is debatable (15).

Protein analyses showed that membrane vesicles isolated using anti-IgE or anti-Thy1 were highly enriched in constituents that preferentially associate with each of these distinct signaling proteins. It is particularly remarkable to have such good separation of FcεRI and Thy-1, because they are both exceptionally abundant constituents of RBL-

2H3 membranes. There are ~200,000 FcεRI molecules and 1 million Thy-1 molecules per cell. Conditions were carefully chosen for cross-linking that favored the formation of very large rafts (300–500 nm in diameter) and minimized the presence of contaminating lipids in the much smaller (~100 nm) vesicle preparations.

Cholesterol was found as the major lipid constituent of FcεRI domains. On a molar ratio, it was roughly equivalent to the combined total of all of the fatty acids extracted from immunisolated FcεRI vesicles. In contrast, the relative concentrations of cholesterol to fatty acid in the Thy-1 domains were only 0.3–0.5. This may explain previous evidence for greater sensitivity of Thy-1-mediated mast cell activation to cholesterol depletion compared with that of FcεRI activation (22). With lower starting levels of cholesterol, the Thy-1 domains might be expected to deplete faster and more completely during the initial exposure to methyl-β-cyclodextrin (MβCD). An attractive alternative explanation is that the higher levels of sphingolipids, known to bind cholesterol, render FcεRI domains partially resistant to cholesterol depletion. One role for cholesterol is likely to be its ability to promote the close packing of sphingolipid molecules (48), also found to be enriched in the FcεRI domains. Intimate associations between FcεRI and cell surface glycosphingolipids were suggested previously by the work of Pecht and colleagues (49) based upon monoclonal antibodies to mast cell glycosphingolipids that inhibit FcεRI-mediated signaling. An early report by Rivnay and Fischer (50) also reported 2- to 5-fold enrichment of sphingomyelin in lipids bound tightly to receptor-IgE complexes.

Treatment of cells with agents that extract cholesterol, such as MβCD, reduces the recovery of raft components, disrupts caveolae, and prevents the formation of functional coated pits (reviewed in Ref. 51). In our experience, the total cholesterol in plasma membranes of cultured cells varies considerably. Fibroblast cell lines, for example, require significantly longer intervals and higher concentrations of MβCD for the depletion of cells loaded with [³H]cholesterol than do RBL cells (data not shown). Thus, it would be difficult to predict how well the exact ratios measured here would translate to receptors in other cell types. Nevertheless, the much higher concentration of cho-

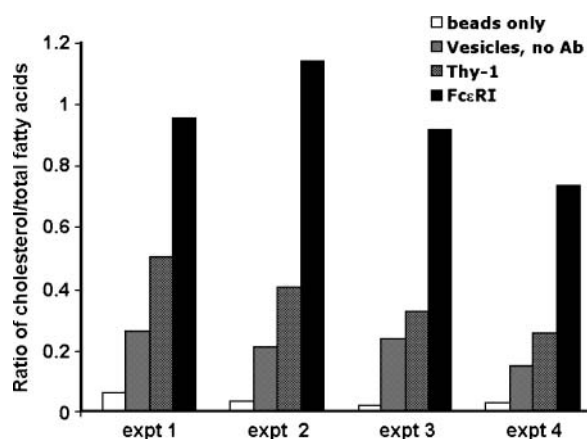



Fig. 8. Measurements of total cholesterol/fatty acid content in FcεRI and Thy-1 microdomains as well as in control samples. Results of four independent experiments are reported. Ab, antibody.

lesterol in FcεRI domains provides unequivocal support for the hypothesis that the IgE receptor and Thy-1 occupy distinct lipid environments in native RBL membranes. A previous study in neuronal membranes found significant differences in lipid composition in immunoprecipitated DRMs of Thy-1 or the GPI-anchored prion protein (52). Compared with Thy-1, that study also found prion protein DRM preparations to have a higher concentration of cholesterol, slightly more unsaturated, longer chain lipids, and 5-fold higher levels of glycosylated hexosylceramide. Morris and colleagues (52) proposed that hydrogen bonding between carbohydrate moieties of glycolipids such as hexosylceramide might affect interactions with prion protein. This theory can obviously apply to many membrane glycoproteins that transiently associate with each other and with glycolipids through weak, non-covalent interactions. Interactions between transmembrane domains likely also influence lipid raft association. Thus, it seems clear that there are a number of mechanisms to explain the considerable heterogeneity in the lipids surrounding specific membrane proteins, regardless of their anchor.

Our analysis of GPE molecular species using isotope-tagged derivatization and nanospray MS³ detection revealed that FcεRI microdomains were also enriched in GPE plasmalogen molecular species relative to the Thy-1 microdomains. Intriguingly, Pike, Han, and Gross (39) also found a relative enrichment in plasmalogens in lipid raft fractions, prepared with and without detergent, compared with postnuclear supernatants. It is worth noting that the vinyl ether linkage at the *sn*-1 position of GPE phospholipids introduces a double bond into the structure that is very near the lipid head group. It is tempting to speculate that this unique feature is preferentially favorable for association with some transmembrane receptors and/or their signaling partners. It is also interesting that the double bonds in GPE plasmalogens, sphingomyelins, and cholesterol are consistent with transmission electron microscopy images of dark patches surrounding aggregated IgE receptors. Sophisticated electron spectroscopy techniques demonstrated that dark patches concentrate osmium, which binds specifically to double bonds in lipids (34). These data suggest that sphingolipids, plasmalogens, and cholesterol are good candidates for the putative lipid shell that may surround some transmembrane receptors (53). Further work is needed to rigorously test this possibility.

Both domains isolated by immunoaffinity chromatography, rather than by sucrose density centrifugation, contain significant amounts of phosphatidylinositols. This is a notable distinction, because Pike, Han, and Gross (39) concluded that phosphatidylinositol appeared to be specifically excluded from raft preparations. Fridriksson et al. (38) did detect phosphatidylinositol in DRM fractions but failed to detect any polyphosphoinositol lipids. Our own study did not extend to the characterization of polyphosphoinositol species within FcεRI domains. We expect that PtdIns(4,5)P₂ and PtdIns(3,4,5)P₃ are present, because our previous electron microscopy studies showed that

receptor signaling patches specifically recruit phospholipase C γ, phosphatidylinositol 3-kinase, and phosphatase with tensin homology on chromosome 10 (36, 54). In addition to its role as substrate for PLCγ and phosphatidylinositol 3-kinase, PtdIns(4,5)P₂ is a critical factor for the recruitment and function of adaptor molecules involved in receptor endocytosis (5), which is initiated in FcεRI signaling domains (36).

The method of purification used here does have an important limitation: it tracks the lipid environment surrounding activated FcεRI receptors, because cross-linking and formation of large signaling patches was an essential feature of the protocol. Thus, evaluation of the local lipid environment for the resting receptor, where receptor clusters are limited to a few receptors and typically have diameters of <20–30 nm (35), remains a technically challenging prospect. It is clear from the work of Brown and colleagues (55, 56) that significant remodeling of lipids occurs during signal transduction. For example, B-cell receptor stimulation leads to significant decreases in overall phosphocholine, phosphatidylinositol, and phosphoethanolamine species and concomitant increases in lysophosphocholine, lysophosphatidylinositol, lysophosphoserine, and glycerophosphatidic acid compounds (56). Similar increases in lysophosphocholine were seen in RBL-2H3 cells within 5 min of antigen stimulation. Future work will explore the nanoscale compartmentalization of lipid components in membranes of both resting and activated cells and the dynamic events associated with localized lipid remodeling during the signaling process. 

The authors thank Dr. Janet Oliver for valuable discussion and Janet Pfeiffer for technical assistance. This work was supported by National Institutes of Health Grants R01 AI-051575 (to B.S.W.) and U54 GM-069338 (to R.C.M.). The University of New Mexico Health Sciences Center Electron Microscopy Facility is gratefully acknowledged.

REFERENCES

1. Melkonian, K. A., T. Chu, L. B. Tortorella, and D. A. Brown. 1995. Characterization of proteins in detergent-resistant membrane complexes from Madin-Darby canine kidney epithelial cells. *Biochemistry*. **34**: 16161–16170.
2. Simons, K., and E. Ikonen. 1997. Functional rafts in cell membranes. *Nature*. **387**: 569–572.
3. Bhatnager, R. S., and J. I. Gordon. 1997. Understanding covalent modifications of proteins by lipids: where cell biology and biophysics mingle. *Trends Cell Biol.* **7**: 14–20.
4. Ilangumaran, S., S. Arni, G. van Echten-Deckert, B. Borisch, and D. C. Hoessli. 1999. Microdomain-dependent regulation of Lck and Fyn protein-tyrosine kinases in T lymphocyte plasma membranes. *Mol. Biol. Cell.* **10**: 891–905.
5. Janes, P. W., S. C. Ley, and A. I. Magee. 1999. Aggregation of lipid rafts accompanies signaling via the T cell antigen receptor. *J. Cell Biol.* **147**: 447–461.
6. Zhang, W., R. Treble, and L. E. Samelson. 1999. Essential role of LAT in T cell development. *Immunity*. **9**: 239–246.
7. Moffett, S., D. A. Brown, and M. E. Linder. 2000. Lipid-dependent targeting of G proteins into rafts. *J. Biol. Chem.* **275**: 2191–2198.
8. Brown, D. A., and J. K. Rose. 1992. Sorting of GPI-anchored proteins to glycolipid-enriched membrane subdomains during transport to the apical cell surface. *Cell*. **68**: 533–544.

9. Horejsi, V., K. Drbal, M. Cebecauer, J. Cerny, T. Brdicka, P. Angelisova, and H. Stockinger. 1999. GPI-microdomains: a role in signalling via immunoreceptors. *Immunol. Today*. **20**: 356–361.
10. Field, K. A., D. Holowka, and B. Baird. 1995. FcεRI-mediated recruitment of p53/56(lyn) to detergent-resistant membrane domains accompanies cellular signaling. *Proc. Natl. Acad. Sci. USA*. **92**: 9201–9205.
11. Montixi, C., C. Langlet, A. M. Bernard, J. Thimonier, C. Dubois, M. A. Wurbel, J. P. Chauvin, M. Pierres, and H. T. He. 1998. Engagement of T cell receptor triggers its recruitment to low-density detergent-insoluble membrane domains. *EMBO J*. **17**: 5334–5348.
12. Cheng, P. C., A. Cherukuri, M. Dykstra, S. Malapati, T. Sproul, M. R. Chen, and S. K. Pierce. 2001. Floating the raft hypothesis: the roles of lipid rafts in B cell antigen receptor function. *Semin. Immunol*. **13**: 107–114.
13. Guo, B. C., R. M. Kato, M. Garcia-Lloret, M. I. Wahl, and D. J. Rawlings. 2000. Engagement of the human pre-B cell receptor generates a lipid raft-dependent calcium signaling complex. *Immunity*. **13**: 2243–2253.
14. Simons, K., and D. Toomre. 2000. Lipid rafts and signal transduction. *Nat. Rev. Mol. Cell Biol*. **1**: 31–40.
15. Edidin, M. 2003. The state of lipid rafts: from model membranes to cells. *Annu. Rev. Biophys. Mol. Struct.* **32**: 257–283.
16. Shogomori, H., and D. A. Brown. 2003. Use of detergents to study membrane rafts: the good, the bad, and the ugly. *Biol. Chem.* **384**: 1259–1263.
17. Mayor, S., and F. R. Maxfield. 1995. Insolubility and redistribution of GPI-anchored proteins at the cell surface after detergent treatment. *Mol. Biol. Cell*. **6**: 929–944.
18. Field, K. A., D. Holowka, and B. Baird. 1999. Structural aspects of the association of FcεRI with detergent-resistant membranes. *J. Biol. Chem.* **274**: 1753–1758.
19. Parolini, I., S. Topa, M. Sorice, A. Pace, P. Ceddia, F. Montesoro, A. Pavan, M. P. Linasanti, C. Peschle, and M. Sargiacomo. 1999. Phorbol ester-induced disruption of the CD4-Lck complex occurs within a detergent-resistant microdomain of the plasma membrane—involverment of the translocation of activated protein kinase C isoforms. *J. Biol. Chem.* **20**: 14176–14187.
20. Surviladze, Z., L. Dráberová, L. Kubínová, and P. Dráber. 1998. Functional heterogeneity of Thy-1 membrane microdomains in rat basophilic leukemia cells. *Eur. J. Immunol.* **28**: 1847–1858.
21. Madore, N., K. L. Smith, C. H. Graham, A. Jen, K. Brady, S. Hall, and R. Morris. 1999. Functionally different GPI proteins are organized in different domains on the neuronal surface. *EMBO J*. **18**: 6917–6926.
22. Surviladze, Z., L. Dráberová, M. Kovářová, M. Bouceik, and P. Dráber. 2001. Differential sensitivity to acute cholesterol lowering of activation mediated via the high-affinity IgE receptor and Thy-1 glycoprotein. *Eur. J. Immunol.* **31**: 1–10.
23. Macdonald, J. L., and L. J. Pike. 2005. A simplified method for the preparation of detergent-free lipid rafts. *J. Lipid Res.* **46**: 11061–11067.
24. Lagerholm, B. C., G. E. Weinreb, K. Jacobson, and N. L. Thompson. 2005. Detecting microdomains in intact cell membranes. *Annu. Rev. Phys. Chem.* **56**: 309–336.
25. Friedrichson, T., and T. Kurzalia. 1998. Microdomains of GPI-anchored proteins in living cells revealed by crosslinking. *Nature*. **394**: 802–805.
26. Varma, R., and S. Mayor. 1998. GPI-anchored proteins are organized in submicron domains at the cell surface. *Nature*. **394**: 798–801.
27. Dietrich, C., B. Yang, T. Fujiwara, A. Kusumi, and K. Jacobson. 2002. Relationship of lipid rafts to transient confinement zones detected by single particle tracking. *Biophys. J.* **82**: 274–284.
28. Bacia, K., I. V. Majoul, and P. Schwille. 2002. Probing the endocytic pathway in live cells using dual-color fluorescence cross-correlation analysis. *Biophys. J.* **83**: 1184–1193.
29. Fujiwara, T., K. Ritchie, H. Murakoshi, K. Jacobson, and A. Kusumi. 2002. Phospholipids undergo hop diffusion in compartmentalized cell membrane. *J. Cell Biol.* **157**: 1071–1081.
30. Kenworthy, A. K., B. J. Nichols, C. L. Remmert, G. M. Hendrix, M. Kumar, J. Zimmerberg, and J. Lippincott-Schwartz. 2004. Dynamics of putative raft-associated proteins at the cell surface. *J. Cell Biol.* **165**: 735–746.
31. Vereb, G., J. Szöllösi, J. Matko, P. Nagy, T. Farkas, L. Vigh, L. Matyus, T. A. Waldmann, and S. Damjanovich. 2003. Dynamic, yet structured: the cell membrane three decades after the Singer-Nicolson model. *Proc. Natl. Acad. Sci. USA*. **100**: 8053–8058.
32. Pike, L. J. 2006. Rafts defined: a report on the Keystone Symposium on Lipid Rafts and Cell Function. *J. Lipid Res.* **47**: 1597–1598.
33. Sanan, D. A., and R. G. W. Anderson. 1991. Simultaneous visualization of LDL receptor distribution and clathrin lattices on membranes torn from the upper surface of cultured cells. *J. Histochem. Cytochem.* **39**: 1017–1024.
34. Wilson, B. S., S. L. Steinberg, K. Liederman, J. R. Pfeiffer, Z. Surviladze, J. Zhang, L. E. Samelson, L. H. Yang, P. B. Kotula, and J. M. Oliver. 2004. Markers for detergent-resistant lipid rafts occupy distinct and dynamic domains in native membranes. *Mol. Biol. Cell*. **15**: 2580–2592.
35. Wilson, B. S., J. R. Pfeiffer, and J. M. Oliver. 2000. Observing FcεRI signalling from the inside of the mast cell membrane. *J. Cell Biol.* **149**: 1131–1142.
36. Wilson, B. S., J. R. Pfeiffer, Z. Surviladze, E. A. Gaudet, and J. M. Oliver. 2001. High resolution mapping reveals distinct FcεRI and LAT domains in activated mast cells. *J. Cell Biol.* **154**: 645–658.
37. Harder, T., P. Scheiffele, P. Verkade, and K. Simons. 1998. Lipid domain structure of the plasma membrane revealed by patching of membrane components. *J. Cell Biol.* **141**: 929–942.
38. Fridriksson, E. K., P. A. Shipkova, E. D. Sheets, D. Holowka, B. Baird, and F. W. McLafferty. 1999. Quantitative analysis of phospholipids in functionally important membrane domains from RBL-2H3 mast cells using tandem high-resolution mass spectrometry. *Biochemistry*. **38**: 8056–8063.
39. Pike, L. J., X. L. Han, and R. W. Gross. 2005. Epidermal growth factor receptors are localized to lipid rafts that contain a balance of inner and outer leaflet lipids. A shotgun lipidomics study. *J. Biol. Chem.* **280**: 26796–26804.
40. Clay, K. L. 1990. Quantitation of platelet-activating factor by gas chromatography-mass spectrometry. *Methods Enzymol.* **187**: 134–142.
41. Hadley, J. S., A. Fradin, and R. C. Murphy. 1988. Electron capture negative ion chemical ionization analysis of arachidonic acid. *Biomed. Environ. Mass Spectrom.* **15**: 175–178.
42. Pulfer, M., and R. C. Murphy. 2003. Electrospray mass spectrometry of phospholipids. *Mass Spectrom. Rev.* **22**: 332–364.
43. Kayganich, K., and R. C. Murphy. 1992. Fast atom bombardment tandem mass spectrometric identification of diacyl, alkylacyl, and alk-1-enylacyl molecular-species of glycerophosphoethanolamine in human polymorphonuclear leukocytes. *Anal. Chem.* **64**: 2965–2971.
44. Zemski Berry, K. A., and R. C. Murphy. 2005. Analysis of cell membrane aminophospholipids as isotope-tagged derivatives. *J. Lipid Res.* **46**: 1038–1046.
45. Harder, T., and M. Kunh. 2000. Selective accumulation of raft-associated membrane protein LAT in T cell receptor signaling assemblies. *J. Cell Biol.* **151**: 199–207.
46. Saucan, L., and G. E. Palade. 1994. Membrane and secretory proteins are transported from the Golgi complex to the sinusoidal plasmalemma of hepatocytes by distinct vesicular carriers. *J. Cell Biol.* **125**: 733–741.
47. van Meer, G. 2005. Cellular lipidomics. *EMBO J*. **24**: 3159–3165.
48. London, E. 2002. Insights into lipid raft structure and formation from experiments in model membranes. *Curr. Opin. Struct. Biol.* **12**: 480–486.
49. Schwartz, A., L. Jurgens, A. Licht, H. Schneider, A. H. Futerman, and I. Pecht. 2000. An IgE-dependent secretory response of mast cells can be induced by a glycosphingolipid-specific monoclonal antibody. *Eur. J. Immunol.* **30**: 217–226.
50. Rivnay, B., and G. Fischer. 1986. Phospholipid distribution in the microenvironment of the immunoglobulin E-receptor from rat basophilic leukemia cell membrane. *Biochemistry*. **25**: 5686–5693.
51. Simons, K., and E. Ikonen. 2000. Cell biology. How cells handle cholesterol. *Science*. **290**: 1721–1726.
52. Brugger, B., C. Grahma, I. Leibrecht, E. Monbelli, A. Jen, F. Wieland, and R. Morris. 2004. The membrane domains occupied by glycosylphosphatidylinositol-anchored prion protein and Thy-1 differ in lipid composition. *J. Biol. Chem.* **279**: 7530–7536.
53. Anderson, R. G. W., and K. Jacobson. 2002. Cell biology. A role for lipid shells in targeting proteins to caveolae, rafts, and other lipid domains. *Science*. **296**: 1821–1825.
54. Gillooly, D. J., and H. Stenmark. 2001. Cell biology. A lipid oils the endocytosis machine. *Science*. **291**: 993–994.
55. Ivanova, P., B. A. Cerda, D. A. Horn, J. S. Cohen, F. W. McLafferty, and H. A. Brown. 2001. Electrospray ionization mass spectrometry analysis of changes in phospholipids in RBL-2H3 mastocytoma cells during degranulation. *Proc. Natl. Acad. Sci. USA*. **98**: 7152–7157.
56. Forrester, J. S., S. B. Milne, P. T. Ivanova, and H. A. Brown. 2004. Computational lipidomics: a multiplexed analysis of dynamic changes in membrane lipid composition during signal transduction. *Mol. Pharmacol.* **66**: 813–821.